

## Nonlinear THz response of a one-dimensional superlattice

Avik W. Ghosh\* and John W. Wilkins

*Department of Physics, 174 West 18th Avenue, Ohio State University, Columbus, Ohio 43210*

(Received 17 February 1999; revised manuscript received 12 August 1999)

The dynamics of an electron in a one-dimensional superlattice is investigated under the action of a THz electric field. The density matrix equations of motion within a single miniband are solved using a relaxation-time approximation for scattering. The electronic response to THz radiation is obtained by calculating the dipole moment, whence we compute the power dissipated, the THz reflection coefficient and dipole radiation. Collisions are essential in eliminating transients and bringing the electron in phase with the field at dynamic localization. The optical properties of the superlattice bear strong signatures of dynamic electron localization such as oscillations with varying field strengths. In addition, the response is multivalued in the incident field owing to the nonlinear relation between the incident and internal fields of the superlattice. The optical properties are robust with respect to the inclusion of higher harmonics, weak collisions, and deviations from a tight-binding miniband dispersion.

### I. INTRODUCTION

Recently, there has been considerable theoretical and experimental progress in studying the dynamics of charges in a semiconductor superlattice in response to intense ultrafast external fields. Following the suggestions of Esaki and Tsu,<sup>1</sup> fabrication of semiconductor superlattices with atomic level precision is now routinely achieved. In a superlattice, the large periodicity ( $\sim 100$  Å) of the multiple quantum well potential makes the minibandwidth much smaller ( $\sim 1$  meV) than the bulk semiconductor bandwidth ( $\sim 1$  eV). This means that a modest electric field of around 10 KV/cm can accelerate electrons to the band edge faster than the average electronic collision time ( $\sim 1$  ps). The driven electrons in the superlattice can then respond to the nonparabolic miniband dispersion at the band edge by exhibiting a host of nonlinear optical properties, which would otherwise be masked by collision-induced drifts in bulk semiconductors. In this paper, we analyze some consequences of the nonlinear response, in particular Bloch oscillations and dynamic localization.

Central to Bloch oscillation phenomena<sup>2,3</sup> is a DC external field  $E_0$  on a particle in a periodic potential (period  $d$ ), with a relaxation rate that is slower than the Bloch oscillation frequency  $\omega_B = eE_0d/\hbar$ . The electron is then localized by the driving field and Bloch oscillates at  $\omega_B$ . Bloch oscillations of electrons in superlattices and their energy domain counterpart—Wannier-Stark ladders, have been observed experimentally using a host of nonlinear optical techniques. The existence of Bloch oscillations has even been confirmed up to room temperature.<sup>4</sup> In addition, Bloch oscillations have been demonstrated in other periodic systems such as for quasicharges in Josephson junctions<sup>5</sup> and dilute gas atoms in optical potentials<sup>6</sup>, and their existence predicted in the motion of magnetic solitons in anisotropic spin-half chains.<sup>7</sup>

Considerably more dramatic is the prediction that an alternating field that otherwise causes an electron to drift will localize it at a discrete set of field values—a phenomenon known as “dynamic localization.”<sup>8,9</sup> For an ac field  $E(t) = E_1 \cos\omega t$ , the electron dynamics is governed by the param-

eter  $\Theta \equiv eE_1d/\hbar\omega \equiv \omega_B^{AC}/\omega$ , where  $\omega_B^{AC}$  is the ac Bloch oscillation frequency. When this parameter  $\Theta$  is a root of the zeroth order Bessel function, the electron is predicted to execute bounded ac Bloch oscillations, else it drifts off. This behavior is easily understood in terms of a simple semiclassical picture;<sup>10</sup> the electron continues to execute ac Bloch oscillations in phase with the incident field if it manages to complete an integer number of oscillations in half an ac period (i.e., before the field switches sign). If the incident and ac Bloch frequencies are not synchronized however, the mismatch causes the electron to drift off. The dynamic localization is expected to persist, albeit modified, in the presence of multibands,<sup>11</sup> scattering,<sup>12</sup> and other nonlinearities.<sup>13</sup>

Theory has so far failed to identify a direct experimental realization of dynamic localization in superlattices. In transport measurements with photon-assisted tunneling, the appearance of absolute negative conductance has been attributed to dynamic localization.<sup>14</sup> In addition, dynamic localization is expected to suppress the dc component of an incident dc-ac field, which has also been experimentally observed.<sup>15</sup> However, the experience with Bloch oscillations argues for a more direct measurement of dynamic localization. One reason why such a measurement has been elusive so far is the high frequency and power requirements that the incident field has to satisfy if the dynamic localization is to dominate over collision effects. The collision time restriction requires the incident frequency to be in the THz regime. At such high frequencies the generation, propagation, and detection of coherent radiation can only be done optically. With the recent availability of free electron lasers as THz sources, the ability to spatially combine inputs to and outputs from superlattices in a quasioptical setup,<sup>16</sup> and ultrafast detectors, one should anticipate the direct observation of dynamic localization. With this in mind, we analyze the nonlinear optical response of a superlattice in an intense THz field.

The organization of the paper is as follows. In Sec. II, we write down the density matrix equations of motion for an electron in a superlattice under the action of a THz field. The electronic dipole moment of an electron exhibits Bloch oscillations in a dc field, and dynamic localization in an ac

field. In Sec. III, we discuss the importance of collisions, both in eliminating the transient response and in enabling power dissipation. The reflection coefficient is calculated in Sec. IV, which demonstrates oscillations as a function of the electric field, associated with dynamic localization. Multistability effects arising from nonlinear penetration of the incident field into the superlattice are dealt with in Sec. V. Section VI deals with dipole radiation, which can be channelized into a few frequency modes by simply tuning the field amplitudes. Finally, in Sec. VII we discuss the corrections to our model due to higher harmonic feedback, collisions and nontight-binding miniband dispersion.

## II. DIPOLE MOMENT

Focussing on the dipole moment leads to both an efficient derivation and a straightforward interpretation of the nonlinear optical properties. For a one-dimensional, one miniband superlattice with growth direction  $z$  (also the direction of the incident THz electric field), the dipole matrix element  $\hat{\mu}_{kk'}$  is defined in terms of electron wave functions in the superlattice  $\Psi_k(z)$ :

$$\hat{\mu}_{kk'} \equiv e \int_{-\infty}^{\infty} dz \Psi_{k'}^*(z) z \Psi_k(z). \quad (1)$$

The superlattice wave function  $\Psi_k(z)$  can be written in an envelope-function approximation as a superposition of wave functions localized at the quantum wells modulated by a plane wave. The wave functions may be approximated by sinusoids in the wells and decaying exponentials in the barriers. Assuming overlap between nearest-neighboring wells only, the dipole matrix element then simplifies to

$$\hat{\mu}_{kk'} = \frac{ie}{\hbar} \frac{\partial}{\partial k} \delta_{kk'}. \quad (2)$$

This form is the same as in a bulk semiconductor. The derivatives of the Kronecker delta will appear only in conjunction with a sum over the quasimomentum.

The dipolar interaction of the electron with the electric field in the superlattice is described by the Hamiltonian

$$\hat{H} = \sum_k \epsilon_k c_k^\dagger c_k - E(t) \sum_{kk'} \hat{\mu}_{kk'} c_k^\dagger c_{k'}, \quad (3)$$

where  $c^\dagger$  and  $c$  are the electron creation and destruction operators, respectively. For a one-dimensional superlattice of period  $d$ , the conduction miniband energy  $\epsilon_k$  approximately follows a tight-binding dispersion  $\epsilon_k = -(\Delta/2)\cos(kd)$ ,<sup>17</sup> the miniband width  $\Delta$  depending on the coupling between neighboring quantum wells. The typical interminiband separation, 80 meV, substantially larger than laser energies ( $\sim 10$  meV), justifies a one miniband assumption. Electrons can be introduced into the conduction miniband either by photoexcitation, or by doping (in the case of doping, additional complications could arise due to domain formation.<sup>18</sup> At THz frequencies, however, the electrons are driven faster than the typical domain formation rate, so we ignore domains hereafter).

The nonlinear optical properties associated with electrons in the conduction miniband subjected to a high frequency electric field are effectively described by the time-dependent

density matrix. In terms of the ‘‘center of mass’’ coordinate  $K \equiv (k+k')/2$  and ‘‘relative’’ coordinate  $q \equiv k-k'$ , this reads

$$N_{Kq} = \langle c_{K+q/2}^\dagger c_{K-q/2} \rangle. \quad (4)$$

The Hamiltonian (3) allows us to compute the time evolution of the density matrix<sup>19</sup>

$$\frac{\partial N_{Kq}}{\partial t} = i \frac{(\epsilon_{K+q/2} - \epsilon_{K-q/2})}{\hbar} N_{Kq} - \frac{eE(t)}{\hbar} \frac{\partial N_{Kq}}{\partial K}. \quad (5)$$

The equation for the diagonal component ( $q=0$ ) above is identical in form to the semiclassical Boltzmann transport equation for the electron distribution function, except for a collision integral on the right-hand side. We include the collision through a relaxation-time approximation. As we shall see, the collisions are important in dropping the transient electromagnetic response of the superlattice electrons.

An important corollary to the density matrix equation is the acceleration theorem for a single miniband in absence of collisions,  $\hbar dK/dt = eE(t)$ . This equation turns out to be the equation for the characteristic curves<sup>21</sup> of Eq. (5) along which the density matrix  $N_{Kq}(t)$  is stationary. Note that in our analyses we are using a semiclassical approximation, which is justified for a superlattice since the wavelength of the field ( $\sim 0.1$  mm for a THz pulse) is much larger than the typical length of a superlattice ( $\sim 1 \mu\text{m}$ ).

In terms of the time-dependent density matrix describing the distribution of electrons in the quasimomentum  $k$  space, the ensemble-averaged electronic dipole moment is then given by

$$\mu(t) = \text{Tr}(\hat{\mu}N) = -\frac{ie}{\hbar} \sum_K \left[ \frac{\partial N_{Kq}(t)}{\partial q} \right]_{q=0}. \quad (6)$$

Using Eqs. (5) and (6), we verify that the above form of the dipole moment satisfies the following equation:<sup>20</sup>

$$\frac{\partial \mu}{\partial t} + \frac{\mu}{\tau} = e \sum_K v_K N_{K0}(t), \quad (7)$$

where  $v_K \equiv \partial \epsilon_K / \partial (\hbar K)$  is the band velocity of the electrons. Note that the dipole moment  $\mu$  depends only on the diagonal ( $q=0$ ) components of the density matrix, i.e., on the electronic distribution function.

The various experimentally realizable nonlinear responses can now be illustrated for simple models of dipole dynamics: free electron and tight-binding dispersions in dc and ac electric fields. The initial distribution of the electron is assumed to be Gaussian in  $K$ , centered around  $k_0$  with a width  $\sigma$ . We solve the density matrix Eq. (5) using the method of characteristics<sup>21</sup> and then use Eq. (7) to get the dipole moment. The following simple cases summarize the variety of nonlinear responses to different time-dependent fields in the absence of collisions ( $\tau = \infty$ ):

(i)  $E=0$ , *free electron*: The electron simply moves at a constant velocity fixed by the initial quasimomentum of the center of the wave-packet:  $\mu(t) = ev_{k_0} t$ .

(ii)  $E=0$ , *tight-binding miniband*: Here too, the electron shows a steady drift:  $\mu(t) = ev_{k_0} t \exp[-\sigma^2 d^2/2]$ . For an

electron with a narrow initial distribution function, the initial quasimomentum  $k_0$  is well defined, and the drift is linear in time.

(iii) *dc field*  $E=E_0$ , *free electron*: The electron accelerates under the influence of the electric field, so the dipole moment increases quadratically with time:

$$\mu(t) = \frac{\Delta d^2}{4E_0} \left[ \left( k_0 + \frac{eE_0 t}{\hbar} \right)^2 - k_0^2 \right] \quad (8)$$

(iv) *dc field*  $E=E_0$ , *tight binding*: An initially localized electron exhibits Bloch oscillations in a dc field at a frequency  $\omega_B = eE_0 d/\hbar$ :

$$\mu(t) = \frac{\Delta}{2E_0} e^{-\sigma^2 d^2/2} [\cos(k_0 d) - \cos(k_0 d + \omega_B t)]. \quad (9)$$

One can also see that the amplitude of the Bloch oscillations is inversely proportional to the field. A stronger field thus tends to localize the electron, while at the same time causing it to oscillate faster. Moreover, if we excited an initial distribution of carriers around the miniband center ( $k_0 \approx \pm \pi/2d$ ), the net dipole moment of the system vanishes because the individual contributions around  $\pm k_0$  oscillate at  $\omega_B$  out of phase with each other. The electronic center of mass does not Bloch oscillate under these circumstances, but the envelope expands and contracts at the Bloch frequency generating a ‘‘breathing mode.’’<sup>3</sup>

(v) *ac field*  $E=E_1 \cos(\omega t)$ , *tight binding*: The electron now exhibits dynamic localization.<sup>9</sup> The dipole moment has a term linear in time corresponding to a uniform drift, and an additional bounded oscillating term arising from ac Bloch oscillations. The linearly growing term bears a Bessel prefactor, which controls the localization properties of the electron. If  $\Theta = eE_1 d/\hbar \omega$  is a root of the Bessel function, then we are left with the oscillating part of the dipole moment, and the electron is dynamically localized

$$\begin{aligned} \mu_t(t) = & \frac{\Delta e d}{2\hbar} e^{-\sigma^2 d^2/2} [\sin(k_0 d) (t J_0(\Theta) + A_u(t)) \\ & - A_v(t) \cos(k_0 d)], \end{aligned} \quad (10)$$

where  $A_u(t)$  and  $A_v(t)$  are given by a superposition of harmonics

$$\begin{aligned} A_u(t) & \equiv 2 \sum_{p=1}^{\infty} \frac{J_{2p}(\Theta)}{2p\omega} \sin(2p\omega t) \\ A_v(t) & \equiv 2 \sum_{p=0}^{\infty} \frac{J_{2p+1}(\Theta)}{(2p+1)\omega} \cos[(2p+1)\omega t]. \end{aligned} \quad (11)$$

In presence of collisions, the dipole moment  $\mu_t(t)$  corresponds, as we shall see, to a transient term. The time evolution of  $\mu_t(t)$  is seen in the graphs in Fig. 1 at small times ( $t \ll \tau$ ). We set the incident angular frequency  $\omega = 1$  THz and the collision time  $\tau = 10$  ps and vary  $\Theta$  by varying the field amplitude  $E_1$ . For the dashed curves, the electron is in the middle of a Bloch oscillation when the field switches sign, so the response is a drift. At dynamic localization (solid curves) however,  $\Theta$  is a root of the zeroth order Bessel function. For the corresponding field values the electron is now complet-

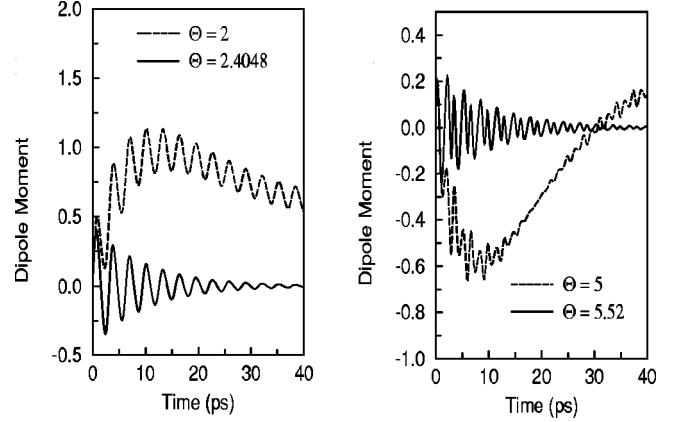


FIG. 1. Effect of ac electric field on the electronic dipole moment  $\mu(t)$  plotted versus time for varying values of  $\Theta = eE_1 d/\hbar \omega$ . We set  $\omega = 1$  THz,  $\tau = 10$  ps, with an initial Gaussian distribution centered around  $k_0 = \pi/2d$ . The solid lines describe dynamic localization while the dotted lines correspond to motion away from dynamic localization. At small times ( $t \ll \tau$ ) the dipole moment grows linearly in time except at dynamic localization where an integer number of ac Bloch oscillations (one in the left graph, two on the right) are completed in half an AC period, and the motion is oscillatory [Eq. (10)]. For large times ( $t \gg \tau$ ) the steady-state dipole moment is oscillatory in general, but vanishes at dynamic localization [Eq. (12)].

ing an integer number of Bloch oscillations in half an ac period ( $\sim 3.14$  ps), and exhibits bounded ac Bloch oscillations.

### III. ROLE OF COLLISIONS

Collisions are crucial both in eliminating the transient response and in enabling power dissipation. Equation (10) for the dipole moment in an ac field was derived in the collisionless limit ( $\tau = \infty$ ). The corresponding dipole moment conforms to the heuristic description of dynamic localization in the Introduction. Introducing collisions through a relaxation-time approximation leads to a transient and a steady-state response in the solution to the density matrix equation. While dc Bloch oscillation is a *transient* phenomenon observed only within the relaxation-time  $\tau$ , dynamic localization is a *steady-state* response, observed beyond the relaxation time, as energy is pumped into the system. For the steady-state ac response therefore, we must first drop the transient response (10), which persists for about a picosecond, and then take a weak collision limit ( $\omega \tau \rightarrow \infty$ ) over the pulse length ( $\sim 1 \mu s$ ). This yields the steady-state dipole moment

$$\begin{aligned} \mu_{ss}(t) = & \frac{\Delta e d}{2\hbar} e^{-\sigma^2 d^2/2} J_0(\Theta) \{ \sin(k_0 d) [ \tau J_0(\Theta) + A_u(t) ] \\ & - A_v(t) \cos(k_0 d) \}. \end{aligned} \quad (12)$$

In contrast to expression (10), the steady-state expression above has an overall Bessel renormalization factor, which causes the dipole moment to vanish completely at dynamic localization (solid lines in Fig. 1 at times  $t \gg \tau$ ). The time-dependent dipole moment at arbitrary times is given by a

mixture of the transient response (10) and the steady-state response (12) (plotted in Fig. 1)

$$\mu(t) = \mu_t(t)e^{-t/\tau} + \mu_{ss}(t)(1 - e^{-t/\tau}) - \frac{\Delta e d}{2\hbar} J_0^2(\Theta) \sin(k_0 d) t e^{-t/\tau} e^{-\sigma^2 d^2/2}. \quad (13)$$

For small times ( $t \ll \tau$ ), the transient response (10) dominates, while at large times ( $t \gg \tau \gg 2\pi/\omega$ ), we get the steady-state response (12). In the following, we assume a momentum-independent initial electronic distribution between  $\pm k_F$ . This corresponds to setting  $k_0 = 0$  above, and replacing  $\exp[-\sigma^2 d^2/2]$  by  $\sin(k_F d)/k_F d$ . We will absorb this factor in the overall electron density  $n$ . The steady-state dipole moment then assumes the form described in Ref. 20.

The steady-state current density can be obtained in the weak-collision limit by differentiating the dipole moment with respect to time and multiplying by the electron density  $n$

$$j(t) = \frac{ned\Delta}{2\hbar} J_0(\Theta) \sin(\Theta \sin \omega t). \quad (14)$$

This form is the same as obtained by Ignatov *et al.*<sup>22</sup> and Holthaus,<sup>23</sup> namely, proportional to the electron density  $n$  and the instantaneous band velocity, but with the overall Bessel renormalization term. The Bessel factor arises exclusively out of the act of dropping the transient response (terms  $\propto \exp[-t/\tau]$ ). Note that the above current density is *out of phase* with the incident field in the weak-collision approximation.

The power dissipated in the superlattice, however, depends on the component of the current density *in phase* with the external field. In other words, we need to retain the leading collisional corrections to the current density in Eq. (14) instead of taking the collisionless limit. In terms of the effective mass  $m^* \equiv 2\hbar^2/\Delta d^2$  of the electrons at the bottom of the conduction miniband, the dissipated power turns out to be<sup>22,24</sup>

$$P \equiv \frac{\omega}{2\pi} \int_0^{2\pi/\omega} j(t) E_1 \cos(\omega t) dt = \frac{n\hbar^2}{m^* d^2 \tau} [1 - J_0^2(\Theta)]. \quad (15)$$

At low-field values ( $\Theta \ll 1$ ), the above power dissipation approximates to the Drude limit  $ne^2 E_1^2 / 2m^* \omega^2 \tau$ , which corresponds to a quadratic rise with the field. At large field values, the power dissipation saturates to a field independent value  $n\hbar^2 / m^* d^2 \tau = n\Delta / 2\tau$  determined by the average energy absorbed between two successive collisions by the electrons from the field.

The power dissipation varies with the electric field in a manner shown in Fig. 2. The initial quadratic rise as predicted by the Drude model is shortly replaced by a saturation, with oscillations reaching maximum at the Bessel roots. This may seem counterintuitive, since dynamic localization implies a small current, and in particular, zero current for  $t \gg \tau$ . The explanation lies in the relative behaviors of current components in-phase and out of phase with the electric field (Fig. 3). The component of the current density in phase with the field is typically  $1/\omega\tau$  times weaker than the out-of-phase

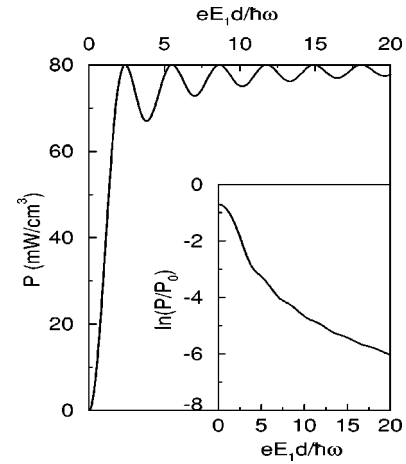


FIG. 2. Power dissipated in a superlattice, plotted versus the parameter  $\Theta = eE_1 d / \hbar \omega$ . At low-field values, the dissipation is quadratic in the field, as predicted by the Drude model. At higher fields, the nonlinear response of the electron causes the dissipation to oscillate as it approaches saturation. The dissipation is maximum at dynamic localization, which occurs when  $\Theta$  is a root of the zeroth order Bessel function. At these values the current is in phase with the incident field. *Inset*: The decay length of the signal, plotted versus  $\Theta$ . This is often the physically measured quantity (except for an overall minus sign). While the dissipated power saturates with high field, the incident power  $P_0$  grows quadratically with the incident field. Thus, the decay length drops drastically with increasing field, and the oscillations due to the Bessel functions form small ripples on it.

term, and is zero in the collisionless limit. At dynamic localization, the larger out-of-phase component diminishes, leading to an overall reduction in the current. However, the in-phase component actually increases, since the electron now comes into phase with the electric field (recall the heuristic description of dynamic localization in the Introduction). In

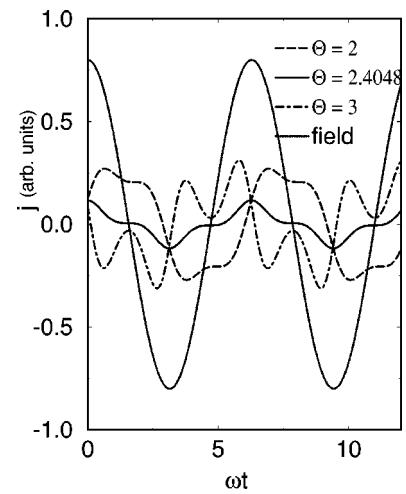


FIG. 3. Current density plotted versus time for different values of  $\Theta = eE_1 d / \hbar \omega$ , along with time-dependence of the (cosine) THz field, for  $\omega\tau = 10$ . Notice that over one period, the average current density is in general zero. However at dynamic localization ( $\Theta = 2.4048$ ), the current density drops in amplitude but comes in phase with the incident field, so the average current density is no longer zero. Thus, dynamic localization decreases the overall current density while increasing the dissipation.

other words, *dynamic localization causes the electrons to localize, and at the same time to come into phase with the incident field*. This diminishes the current while at the same time increasing the dissipation.

In most experiments however, the physically measured quantity is the decay length, defined as the distance over which the incident power  $P_0$  decays by a factor  $1/e$ . The incident power is quadratic in  $\Theta$ , while the dissipated power approaches saturation at high fields  $\Theta$ . Hence the decay length  $\sim \ln(P/P_0)$  decreases drastically with the field (inset in Fig. 2). This washes out the Bessel oscillations, which only appear as ripples on the sharply decreasing background.

#### IV. REFLECTION COEFFICIENT

In contrast to the decay length, the THz reflection coefficient of the superlattice turns out to be a more sensitive probe of dynamic localization. We analyze the reflection of the superlattice in terms of an effective dielectric function  $\epsilon_{\text{eff}}(\Theta)$  obtained from the coefficient of the first harmonic term in Eq. (12) for  $k_0=0$ . This corresponds to a linear response analysis in the time dependence  $\cos(\omega t)$ , not in the field  $\Theta$ . Taking into account the background dielectric constant  $\epsilon_0 \approx 12.9$  of the GaAs substrate, we have<sup>20</sup>

$$\epsilon_{\text{eff}}(\Theta) = \epsilon_0 \left[ 1 - 2 \frac{\omega_p^2}{\omega^2} \frac{J_0(\Theta)J_1(\Theta)}{\Theta} \right]. \quad (16)$$

The electronic response appears through the part involving the plasma frequency  $\omega_p \equiv \sqrt{4\pi n e^2 / m^* \epsilon_0}$ . For  $\Theta \ll 1$ , the ‘‘linear response’’ regime, the above dielectric function reduces to that for three-dimensional (3D) plasmons. We compute the reflection coefficient derived from the above nonlinear dielectric function.<sup>25</sup>

The reflection coefficient as a function of  $\Theta$  has been computed in Ref. 20 for  $\omega_p/\omega=8$  (for a superlattice with period 100 Å, miniband width 18 meV, and an incident angular frequency  $2\pi \times 1$  THz, this corresponds to an electron density  $\sim 7.5 \times 10^{11}$  cm<sup>-2</sup> per well). At low fields, plasmons screen the field in the superlattice leading to total reflection, while at high fields the reflection reaches the background dc value as the plasmon screening becomes ineffective. Strikingly the reflection coefficient exhibits prominent oscillations around the background, matching the background value at dynamic localization, dictated by the roots of the two Bessel functions in Eq. (16). In fact, the first root is in the total reflection regime, so there is a window of low reflection in the otherwise high reflectivity zone. So strong is the nonlinear response due to dynamic localization that it completely overwhelms the plasmon screening.

In computing the above reflection coefficient, we have restricted ourselves to one miniband and deliberately dropped the higher harmonics. One way of incorporating the contributions of the higher harmonics is to use a method suggested by Broer for an arbitrary nonlinearity.<sup>26</sup> The result exhibits high frequency wiggles on top of the reflection graph calculated in Ref. 20, as well as a shift in the zeros of the reflection from the roots of the higher order Bessel functions.<sup>24</sup> The overall field dependence of the reflection coefficient is thus hardly affected by the inclusion of higher harmonics.

#### V. OPTICAL BISTABILITY

The nonlinear response also affects the way the incident field penetrates into the superlattice, and turns out to be the cause for optical bistability in the system. Moreover, the response does not compartmentalize naturally into exclusively propagating or decaying waves in the medium. For a high-electron density (large  $\omega_p$ ) the nonlinear penetration involves a transformation that makes the field  $E_S$  inside the superlattice a multivalued function of the incident field  $E_I$ . The electron responds directly to the local field inside the superlattice. In order to make contact with experiments, we will first need to make a variable transformation from  $E_S$  to  $E_I$ . This transformation is nonlinear, and makes the local field a multivalued function of the incident field.

The variables  $E_S$  and  $E_I$  are connected via boundary conditions at the surface  $x=0$ , where  $x$  is the propagation direction of the THz wave. The boundary conditions are obtained by matching tangential components of electric and magnetic fields at the superlattice surface. The  $x$ -dependence of  $\Theta_S(x) = eE_S d / \hbar \omega$  is obtained by writing down the wave equation inside the superlattice, ignoring higher harmonics as before.<sup>20</sup> The prominent field-dependences are

(a) *propagating*,  $\epsilon_{\text{eff}}(\Theta_0) = 0$ . Here, the amplitude is constant with respect to  $x$ , so  $|\Theta_S(x)| = |\Theta_S(0)| = \Theta_0$ . The wave equation then gives us the familiar propagation condition  $\epsilon_{\text{eff}}(\Theta_0) > 0$ , where  $\Theta_0 = \Theta_S(0)$ ;

(b) *decaying*,  $\int_0^{\Theta_S(x)} y \epsilon_{\text{eff}}(y) dy < 0$ . For a decaying wave,  $|\Theta_S(x)| = \Theta_S(x)$  as far as position-dependence is concerned. The wave equation then assumes the form

$$\frac{d^2 \Theta_S(x)}{dx^2} = - \left\{ \frac{\omega^2}{c^2} \epsilon_{\text{eff}}[\Theta_S(x)] \right\} \Theta_S(x). \quad (17)$$

The equation can be integrated between  $x$  and infinity, assuming the field decays to zero far into the superlattice, to yield

$$\frac{1}{2} \left[ \frac{d\Theta_S(x)}{dx} \right]^2 = - \frac{\omega^2}{c^2} \int_0^{\Theta_S(x)} y \epsilon_{\text{eff}}(y) dy. \quad (18)$$

The derivative  $d\Theta_S(x)/dx$  should be a real function of  $x$  for a decaying wave, which leads to the self-consistency condition  $\int_0^{\Theta_S(x)} y \epsilon_{\text{eff}}(y) dy < 0$ .<sup>27</sup>

The conditions for propagating and decaying waves in (a) and (b) are neither mutually exclusive, nor exhaustive. *This means that there are certain field  $\Theta_S$  inside the superlattice which support both kinds of waves, and certain other field values which cannot be propagated within the superlattice.* In the special case where  $\epsilon_{\text{eff}}[\Theta_S(x)] = \text{constant}$ , however, conditions (a) and (b) correspond to the two familiar disjoint sectors, viz.,  $\epsilon_{\text{eff}} > 0$  in (a) and  $\epsilon_{\text{eff}} < 0$  in (b).<sup>28</sup>

The solutions to the wave equation in regions (a) and (b), in conjunction with the boundary conditions at the surface, give us the nonlinear transformation  $\Theta_S$  vs  $\Theta_I$ .<sup>20</sup> For a given incident laser power there are multiple solutions for the local field inside the superlattice. Each such local field uniquely determines the electronic response. So the behavior of the electron to a given incident power depends on the branch of the transformation curve that we are sitting on. Incorporating the nonlinear transformation into the reflection coefficient

leads to multistable loops and oscillations in the reflection coefficient as a function of the incident laser power.<sup>20</sup>

## VI. DIPOLE RADIATION

In calculating the optical properties so far, we ignored the higher harmonics in comparison to the fundamental response. If we look at dipole radiation, however, the situation changes completely. Higher harmonics tend to radiate more, since dipole radiated power varies as the fourth power of the dipole oscillation frequency. However, there is a natural cut off for the highest harmonic allowed in the system. This is controlled by the parameter  $\Theta \equiv \omega_B^{AC}/\omega$ , which fixes the maximum number of ac Bloch oscillations in half the period of the incident field.

Operationally, we use Larmor's formula for dipole radiation.<sup>31</sup> This gives us the dipole radiated power as a fraction of the incident power

$$\frac{P_{\text{rad}}}{P_I} = \frac{8\pi}{3A_{\text{spot}}} \left[ N_e \frac{2e^2}{m^*c^2} \right]^2 \frac{J_0^2(\Theta)}{\Theta^2} \sum_{p=0}^{\infty} (2p+1)^2 J_{2p+1}^2(\Theta), \quad (19)$$

where  $A_{\text{spot}}$  is the spot area of the superlattice illuminated by the incident THz radiation, and  $N_e$  is the number of radiating electrons. The above sum is finite; in fact, when the index of a Bessel function is greater than the argument, the Bessel terms decrease exponentially with the index, so harmonics beyond  $(2p+1) \approx \Theta$  do not contribute much to the radiation. This gives us the cut-off harmonic.<sup>24</sup>

Critical in the applicability of Larmor's formula above is the fact that we are using the form for a point dipole. This makes it essential to put the detector at a distance much larger than the wavelength ( $\sim 0.1$  mm) of the THz radiation. The effect of several electrons is included simply by multiplying the individual dipole moment by  $N_e$ . This is true as long as all the electrons are moving coherently in the same direction. However, if the extent of the superlattice along the  $x$  direction is larger than half a THz wavelength for a particular mode, then the electrons in the superlattice will divide into segments moving in opposite directions, and their radiated fields would tend to cancel out. One way to avoid this, while at the same time keeping  $N_e$  reasonably large, would be to inactivate odd half wavelengths of the superlattice by ion-implantation.

Figure 4 shows a plot of the fractional radiated power as a function of  $\Theta$  and the order  $2p+1$  of the harmonics [contributions from individual terms in the sum in Eq. (19)]. From the figure, we see that aside from the fundamental response, maximum dipole radiation occurs in the mode whose order equals the field. In other words, by simply varying the field amplitude, one can cut off the radiation from most harmonic modes, and select out a preferential mode for radiation.

## VII. DISCUSSIONS

We have simplified our model to the idealized case of a set of weakly interacting electrons in a single tight-binding superlattice miniband, responding to a THz plane wave propagating monochromatically into the superlattice. For this system, we have calculated the optical response, including

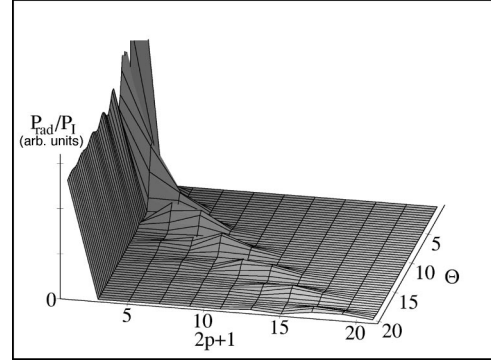


FIG. 4. Dipole radiated power (a.u.) plotted as a fraction of the incident power, versus  $\Theta = eE_1d/\hbar\omega$  and the order  $2p+1$  of the radiating harmonic for  $\omega_p/\omega = 1.2$ . The power radiated at a fixed field increases with harmonics upto a certain order ( $2p+1 \sim \Theta$ ), and then falls off exponentially.

the nonlinear transformation at the boundary. In this section, we consider the effects of relaxing each assumption individually. Our main observation is that the sharpness of our previous results allows the nonlinear effects to persist.

*Feedback effects from higher harmonics.* One of the quantities that may be easier to monitor experimentally as a probe of dynamic localization is the third harmonic generation. This is because the substrate does not contribute to higher harmonic generation; the third harmonic arises exclusively out of the superlattice, which functions as a nonlinear ‘‘inductor,’’<sup>32</sup> in the weak collision limit. The higher harmonics generated propagate through the superlattice and feed back on the fundamental response as well. The third harmonic generation for a series of superlattices in a quasioptical setup also reveals a nonmonotonic dependence on the incident power. The oscillations are related by a nonlinear transformation at the boundary to the roots of the zeroth and third-order Bessel functions. Analogous to the reflection coefficient, the third harmonic power transmitted through the substrate becomes a multivalued function of the incident laser power for high-doping densities.<sup>32</sup> Recent experiments<sup>33</sup> on THz third harmonic generation by a quasioptical array reveal a nonmonotonic field dependence of the generated power. The results are consistent with ac Bloch oscillations followed by Zener tunneling. However, due to significant collisions ( $\omega\tau \lesssim 2$ ), there is no bistability, and the sharpness of the oscillations is severely compromised.

*Collisions.* In all our previous calculations, we have ignored the effects of collisions; the only role of the collisions was to get rid of the transient response. We can introduce collisions through a relaxation-time approximation and retain corrections to  $O(1/\omega^2\tau^2)$ . The effective dielectric function obtained from the dipole moment is then of the form

$$\epsilon_{\text{eff}}(\Theta) = \epsilon_0 \left( 1 - \frac{2\omega_p^2}{\omega^2} \frac{J_0(\Theta)J_1(\Theta)}{\Theta} \left[ 1 - \frac{1}{\omega^2\tau^2} \right] \right) \quad (20)$$

to leading order in  $1/\omega^2\tau^2$  (actually, there is also a shift in phase introduced by collisions, so the fundamental response of the dipole moment has both a sine and a cosine term in its response). The principal effects of such corrections are to diminish the strengths of the oscillations in the reflection

coefficient as the field increases, as well as in diminishing the regime of validity of linear response and plasma screening.<sup>24</sup>

*Non tight-binding miniband.* Deviations from a tight-binding dispersion require a simple extension of our calculations. Let us generalize the tight-binding structure by including couplings over next-nearest-neighboring quantum wells and so on:

$$\epsilon_k = - \sum_{p=1}^{\infty} \frac{\Delta_p}{2} \cos(pkd). \quad (21)$$

The corresponding steady-state dipole moment then has the form

$$\mu(t) = - \sum_{p=1}^{\infty} \frac{e dp \Delta_p}{\hbar \omega} J_0(\Theta_p) \sum_{m=odd}^{\infty} \left[ \frac{J_m(\Theta_p)}{m} \right] \cos m\omega t, \quad (22)$$

where  $\Theta_p = p\Theta$ . Using the above equation in our effective dielectric function as before, we recalculate our reflection coefficient in the presence of non-tight-binding corrections. For definiteness' sake, we make the second nearest neighbor overlap term half as strong as the first ( $\Delta_2 = 0.5\Delta_1$ ), and do not include any longer ranged couplings. The result of the calculation<sup>24</sup> indicates that the appearance of Bessel functions with different arguments in the sum above precludes dynamic localization in its strictest form (vanishing of the dipole moment) from occurring for a non-tight-binding system.<sup>9</sup> In addition to the oscillations described earlier,<sup>20</sup> there are additional oscillations arising out of the Bessel functions with different arguments. However, some of the sharp features such as plasmon screening, oscillations, periodic vanishing of the THz reflection, and multistability in the optical response still survive this band-structure generalization.

*Multiple minibands.* Considerably more serious is the influence of Zener tunneling. As discussed in Refs. 11, 34, and

35, Zener tunneling transports a substantial fraction of the electrons across the minigap at the end of each ac Bloch oscillation. The transfer is large when the separation of the minibands is comparable to the ac Bloch frequency (in the quasienergy picture of Holthaus,<sup>23</sup> this corresponds to avoided crossings of two quasienergy minibands of different indices). This will undoubtedly affect the electronic current, which now has contributions from multiple minibands. However, the interminiband separation is typically around 80 meV, so Zener tunneling is avoidable as long as the incident frequency or the field energy are smaller and significantly off resonance.

## VIII. CONCLUSIONS

In the presence of time-dependent optical fields on a periodic system with a nonparabolic band dispersion and weak collisions, a particle is expected to exhibit a host of optical properties that are nonlinear functions of the input fields. In addition, if we take into account the way the field penetrates into the system from outside, the nonlinear response makes the optical properties multivalued functions of the incident powers. We have demonstrated a variety of effects that bear distinct signatures of such nonlinear response and multistability. In particular, we show that dynamic localization of electrons in a superlattice in the presence of a THz incident field leads to dramatic optical features, which should be observable experimentally.

## ACKNOWLEDGMENTS

This work has been supported by the Office of Naval Research, the Department of Energy, and the Ohio State University Presidential Fellowship. We wish to thank A. V. Kuznetsov, C. J. Stanton, C. Jayaprakash, S. J. Allen, M. C. Wanke, D. D. Awschalom, D. W. Hone, D. S. Citrin, and J. H. Davies for suggestions and helpful discussions.

\*Permanent address: 166 E. Stadium Ave., Apt. #A, West Lafayette, IN 47906.

<sup>1</sup>L. Esaki and R. Tsu, IBM J. Res. Dev. **14**, 61 (1970).

<sup>2</sup>F. Bloch, Z. Phys. **52**, 555 (1929).

<sup>3</sup>A. M. Bouchard and M. Luban, Phys. Rev. B **52**, 5105 (1995).

<sup>4</sup>C. Waschke, H. G. Roskos, R. Schwedler, K. Leo, H. Kurz, and K. Köhler, Phys. Rev. Lett. **70**, 3319 (1993); T. Dekorsy, P. Leisching, K. Köhler, and H. Kurz, Phys. Rev. B **50**, 8106 (1994); T. Dekorsy, R. Ott, H. Kurz, and K. Köhler, *ibid.* **51**, 17 275 (1995).

<sup>5</sup>G. Y. Hu and R. F. O'Connell, Phys. Rev. B **47**, 8823 (1993); L. S. Kuzmin and D. B. Haviland, Phys. Rev. Lett. **67**, 2890 (1991).

<sup>6</sup>M. BenDahan, E. Peik, J. Reichel, Y. Castin, and C. Solomon, Phys. Rev. Lett. **76**, 4508 (1996).

<sup>7</sup>J. Kyriakidis and D. Loss, Phys. Rev. B **58**, 5568 (1998).

<sup>8</sup>F. G. Bass and A. P. Tetervov, Phys. Rep. **140**, 237 (1986).

<sup>9</sup>D. H. Dunlap and V. M. Kenkre, Phys. Rev. B **34**, 3625 (1986).

<sup>10</sup>D. H. Dunlap and V. M. Kenkre, Phys. Lett. A **127**, 440 (1988).

<sup>11</sup>J. Rotvig, A. P. Jauho, and H. Smith, Phys. Rev. Lett. **74**, 1831 (1995).

<sup>12</sup>D. H. Dunlap and V. M. Kenkre, Phys. Rev. B **37**, 6622 (1988).

<sup>13</sup>D. Cai, A. R. Bishop, N. Groenbech-Jensen, and M. Salerno, Phys. Rev. Lett. **74**, 1186 (1995).

<sup>14</sup>B. J. Keay, S. Zeuner, S. J. Allen, Jr., K. D. Maranowski, A. C. Gossard, U. Bhattacharya, and M. J. W. Rodwell, Phys. Rev. Lett. **75**, 4102 (1995).

<sup>15</sup>S. Winnerl, E. Schomburg, J. Grenzer, H. J. Regl, A. A. Ignatov, K. F. Renk, D. P. Pavel'ev, Yu. Koschurinov, B. Melzer, V. Ustinov, S. Ivanov, S. Schaposchnikov, and P. S. Kop'ev, Superlattices Microstruct. **21**, 91 (1997).

<sup>16</sup>R. A. York and Z. B. Popovic, *Active and Quasioptical Arrays for Solid-State Power Combining* (Wiley, New York, 1997).

<sup>17</sup>G. D. Bastard, *Wave Mechanics Applied to Semiconductor Heterostructures* (Editions de Physique, Les Ulis, France, 1988).

<sup>18</sup>H. T. Grahn, H. Schneider, and K. V. Klitzing, Phys. Rev. B **41**, 2890 (1990); A. Sibille, Phys. Rev. Lett. **64**, 52 (1990).

<sup>19</sup>Note that the first term in the equation has the correct sign, in contrast to Ref. 20.

<sup>20</sup>A. W. Ghosh, A. V. Kuznetsov, and J. W. Wilkins, Phys. Rev. Lett. **79**, 3494 (1997).

- <sup>21</sup>A. N. Tikhonov, A. B. Vasil'eva, and A. G. Sveshnikov, *Differential Equations* (Springer Verlag, Munich, 1980).
- <sup>22</sup>A. A. Ignatov and Yu. A. Romanov, *Phys. Status Solidi B* **73**, 327 (1976).
- <sup>23</sup>M. Holthaus, *Phys. Rev. Lett.* **69**, 351 (1992).
- <sup>24</sup>A. Ghosh, Ph.D. thesis, Ohio State University, 1999.
- <sup>25</sup>J. D. Jackson, *Classical Electrodynamics* (Wiley, New York, 1975), p. 282, Eq. (7.42).
- <sup>26</sup>L. J. F. Broer, *Phys. Rev. Lett.* **4**, 65 (1963).
- <sup>27</sup>Equation (18) allows us to construct the decay profile  $\Theta_S(x)$  in the superlattice. For small  $\Theta_0 = \Theta_S(0)$  in particular, we get an exponentially decaying wave with decay length  $2\pi c/\omega\sqrt{|\epsilon_P|}$  corresponding to plasmon screening.
- <sup>28</sup>There could be other types of solutions for a large nonlinearity (large plasma frequency). One type of continuum solutions, for example, generates *linearly inhomogeneous traveling waves* (Ref. 29). We have concentrated on the two simplest kinds of solutions to the wave equation in our discussions. Note that even for a simpler Kerr nonlinearity [ $\epsilon_{\text{eff}}(\Theta) \propto \Theta^2$ ], the wave propagation problem is quite involved (see for example, Ref. 30 and the discussions in Ref. 24).
- <sup>29</sup>A. E. Kaplan, *IEEE J. Quantum Electron.* **QE-17**, 336 (1981).
- <sup>30</sup>A. E. Kaplan, *Kvant. Elektron. (Moscow)* **5**, 166 (1978) [*Sov. J. Quantum Electron.* **8**, 95 (1978)]; *Quantum Electron. Radiophys.* **22**, 229 (1979).
- <sup>31</sup>J. D. Jackson, *Classical Electrodynamics* (Wiley, New York, 1975), p. 659, Eq. (14.22).
- <sup>32</sup>A. W. Ghosh, M. C. Wanke, S. J. Allen, and J. W. Wilkins, *Appl. Phys. Lett.* **74**, 2164 (1999).
- <sup>33</sup>M. C. Wanke, Ph.D. thesis, University of California at Santa Barbara, 1998.
- <sup>34</sup>X-G. Zhao, W-X. Yan, and D. W. Hone, *Phys. Rev. B* **57**, 9849 (1998).
- <sup>35</sup>J. Rotvig, A. P. Jauho, and H. Smith, *Phys. Rev. B* **54**, 17 691 (1996).